Finding the optimal exchange-correlation functional to describe the excited state properties of push-pull organic dyes designed for thermally activated delayed fluorescence

Cardeynaels, Tom; Paredis, Simon; Deckers, Jasper; Brebels, Sonny; Vanderzande, Dirk; Maes, Wouter; Champagne, Benoît

Published in:
PCCP : Physical Chemistry Chemical Physics

DOI:
10.1039/d0cp02409k

Publication date:
2020

Document Version
Publisher's PDF, also known as Version of record

PCCP

ROYAL SOCIETY OF CHEMISTRY

PAPER

Cite this: *Phys. Chem. Chem. Phys.*, 2020, **22**, 16387

Finding the optimal exchange–correlation functional to describe the excited state properties of push–pull organic dyes designed for thermally activated delayed fluorescence†

Tom Cardeynaels, [abc] Simon Paredis, [bc] Jasper Deckers, [bc] Sonny Brebels, [bc] Dirk Vanderzande, [bc] Wouter Maes [bc] and Benoît Champagne *[a]

Received 4th May 2020,
Accepted 6th July 2020

DOI: 10.1039/d0cp02409k

rsc.li/pccp

To gauge the suitability of an organic dye for thermally activated delayed fluorescence (TADF), its excited state properties are often calculated using density functional theory. For this purpose, the choice of the exchange–correlation (XC) functional is crucial as it heavily influences the quality of the obtained results. In this work, 19 different XC functionals with various amounts of Hartree–Fock (HF) exchange and/or long-range correction parameters are benchmarked *versus* resolution-of-the-identity second-order coupled cluster (riCC2) calculations for a set of 10 prototype intramolecular donor–acceptor compounds. For the time-dependent density functional theory (TD-DFT) calculations, LC-BLYP(ω = 0.20) and M06-2X are the better performing XC functionals when looking at singlet and triplet excitation energies, respectively. For the singlet–triplet energy gap, LC-BLYP(ω = 0.17), LC-ωPBE(ω = 0.17) and a hybrid LC-BLYP(ω = 0.20)/M06-2X method give the smallest mean average errors (MAEs). Using the Tamm–Dancoff approximation (TD-DFT/TDA), the MAEs are further reduced for the triplet vertical excitation energies and the singlet–triplet energy gaps.

1 Introduction

Thermally activated delayed fluorescence (TADF) has gained significant interest since its first application to the field of organic light-emitting diodes (OLEDs) in 2009.[1] The prospect of a more efficient and green light-producing technology has prompted researchers worldwide to investigate the intricate properties of TADF and hundreds of new materials have been designed for this purpose.[2–8] Unlike the phosphorescent emitters applied in the 2nd generation OLEDs, TADF-based OLEDs are emissive from the singlet excited state *via* fluorescence. However, they operate under similar circumstances. Due to spin statistics, the excited states within the active layer of the OLED device are formed in a 75/25 ratio for triplet (T_1) with respect to singlet (S_1) states. These triplet states have to be upconverted to the singlet state to achieve external quantum efficiencies (EQEs) that can compete with those obtained for the phosphorescent counterparts. Reversed intersystem crossing (rISC) allows the triplet excitons to be converted to the singlet state, a process that is facilitated when the two states are close in energy and thermal energy enables to overcome this small energy difference. Since the S_1–T_1 energy gap (ΔE_{ST}) is governed by the overlap between (generally) the highest occupied molecular orbital (HOMO) and the lowest unoccupied molecular orbital (LUMO), efficient rISC is achieved by spatially separating the HOMO and LUMO on the organic emitter molecule, giving rise to charge transfer absorption and emission. This can be achieved by coupling 'donor' (electron-rich) and 'acceptor' (electron-poor) subunits, either directly (giving rise to large steric hindrance) or *via* a spiro or other types of sp^3-hybridized junction.[9–12] Moreover, since we are dealing with spin changes, changing the spin angular momentum has to be paired with a change in orbital angular momentum (spin–orbit coupling, SOC) and this is forbidden between ^{1}CT and ^{3}CT states by the El-Sayed rule[13,14] when they have the same orbital character. To overcome this, a second triplet state (locally excited, LE, or of different CT nature) is required to allow mixing through a process known as vibronic coupling.[15–19]

[a] *University of Namur, Laboratory of Theoretical Chemistry, Theoretical and Structural Physical Chemistry Unit, Namur Institute of Structured Matter, Rue de Bruxelles 61, 5000 Namur, Belgium. E-mail: benoit.champagne@unamur.be*
[b] *Hasselt University, Institute for Materials Research (IMO-IMOMEC), Design & Synthesis of Organic Semiconductors (DSOS), Agoralaan 1, 3590 Diepenbeek, Belgium*
[c] *IMOMEC Division, IMEC, Wetenschapspark 1, 3590 Diepenbeek, Belgium*

† Electronic supplementary information (ESI) available: Signed error plots, detailed information about all TD-DFT and TD-DFT/TDA calculations, optimized geometries, HOMO and LUMO topologies, synthesis procedures, ^{1}H and ^{13}C NMR spectra, UV-VIS and fluorescence and coordinates of the optimized geometries can be found. See DOI: 10.1039/d0cp02409k

Computational chemistry has been instrumental to help resolving the mechanism behind these processes,[18–24] showing that even by considering simple properties like structural parameters, it can help to understand the excited state properties of any given emitter. With density functional theory (DFT), the ground-state geometry optimization of small (<25 atoms) to large (>100 atoms) molecules can be performed at low to moderate computational cost. From this, one can already determine the dihedral angle between the donor and acceptor units, as well as the spatial separation of the frontier orbitals. Adiabatic linear-response time-dependent DFT (TD-DFT) can then be used to investigate the excitation energies of the singlet and triplet states, from which the singlet–triplet energy gap (ΔE_{ST}) can be deduced. Although higher level theoretical calculations do exist, such as the second-order approximate coupled cluster singles and doubles model CC2, the computational cost increases rapidly, as N^x with N a measure of the size of the compound (x = 5 for CC2), making these methods inviable to calculate the excited state properties of larger systems for screening purposes.[25] However, the choice of the exchange–correlation (XC) functional in (TD-)DFT calculations is of crucial importance to obtain accurate and reliable results. Several papers have already described the use of TD-DFT or the Tamm–Dancoff approximation to TD-DFT (TD-DFT/TDA) to obtain accurate results for the first singlet and triplet vertical excitation energies of small organic conjugated compounds[26,27] and larger organic dyes for solar cell applications.[28] In the work of Jacquemin *et al.*,[26] 34 different XC functionals (XCFs) were investigated and benchmarked *versus* excitation energies obtained using high level methods such as MS-CASPT2 [*i.e.*, multi-state complete active space self-consistent field (CASSCF) corrected with second-order perturbation theory], CC2, and CC3 (*i.e.*, approximate coupled cluster singles, doubles, and triples model). Among the best performing functionals in their study are BMK (42% HF exchange) and M06-2X (54% HF exchange). Brückner *et al.*[29] investigated the singlet and triplet excitation energies for the application of singlet fission in organic solar cells using 14 different XC functionals benchmarked against MS-CASPT2 calculations. On top of regular TD-DFT calculations, the Tamm–Dancoff approximation was also assessed. The M06-2X XCF was found to give the best results when TD-DFT singlet excitations are combined with TDA triplet values. Wong *et al.*[28] investigated the behavior of the long-range corrected functional LC-BLYP for different values of the range-separating parameter ω on a series of coumarin dyes for dye-sensitized solar cells. Their results using the B3LYP and modified LC-BLYP functionals were benchmarked *versus* CC2 calculations and the authors concluded that the modified LC-BLYP functional significantly improves the accuracy of the singlet excitation energies with respect to B3LYP. Of particular interest are the works of Huang *et al.*,[30] Penfold,[31] Sun *et al.*,[32] and Moral *et al.*,[33] who investigated the behavior of various functionals for TADF active materials and host materials. The earliest investigation by Huang *et al.*[30] benchmarks a series of XCFs to experimental values. The investigation includes long-range separated functionals, but these were found to severely overestimate the S_1 vertical excitation energy due to the lack of tuning of the range-separated parameters. Moral *et al.*[33] used PBE0 within the TDA to evaluate the S_1 vertical excitation energies with respect to experimental values, not aiming to provide a benchmark but rather to deduce structure–property relationships. Additionally, they employed the so-called double hybrids B2-PLYP and B2GP-PLYP to investigate the effects of non-local exchange and correlation on the excitation energies. Although the double hybrid functionals are noted to have a higher computational cost with similar overall results to their calculations with PBE0, they present a slight improvement for the compounds with a larger charge transfer character. Sun *et al.*[32] and Penfold[31] opted to modify the range-separating parameter in LC-ωPBE and LC-BLYP, respectively. In both works, the calculated excitation energies were benchmarked against experimental values for the singlet excitation energies and singlet–triplet energy gaps. With ω values from 0.14 to 0.20 (given in Bohr^{-1} units throughout the paper) for LC-ωPBE and 0.15 to 0.19 for LC-BLYP, the authors found very small errors (MAE < 0.15 eV) with respect to the experimental values for both properties under investigation.

In this work, the adiabatic TD-DFT method is employed to evaluate the first singlet and triplet excitation energies and the corresponding singlet–triplet energy gaps for a set of 10 compounds (Fig. 1) and a number of functionals from different rungs of a ladder leading to quantum chemical accuracy[34] are tested. Our goal is to find a method with a good trade-off between computational cost and accuracy while being applicable to an as large as possible set of compounds. The 10 compounds were chosen from TADF literature or devised from ongoing work within our groups. They were selected because they span a broad range of experimental (and theoretical) singlet–triplet energy splitting values, together with fluorescence characteristics going all the way from blue to red. Furthermore, the compounds were designed to consist of varying donor and acceptor groups to allow generalization. For compounds **1**, **4**, **5**, **6**, **9**, and **10**, TADF properties have been observed experimentally. For compound **3**, it was shown that no TADF is present. To our knowledge, compounds **2**, **7**, and **8** have not been investigated yet in literature and no experimental data on their TADF behavior are available. The synthesis of compounds **2**, **7**, and **8** is therefore reported, together with their UV-VIS absorption and emission spectra. For the sake of consistency, we carried out similar optical characterizations for the other compounds to provide a data set for comparison with the quantum chemical predictions. Our set of XCFs includes those that were already previously tested with good results, such as M06-2X, LC-BLYP(ω = 0.17), and LC-ωPBE(ω = 0.17), the two latter with modified range-separating parameters. We opted for averages of the optimal ω values obtained by Sun *et al.*[32] and Penfold,[31] because this is more convenient for screening purposes than having to optimize this parameter for every compound, either to get the smallest errors on the excitation energies or to satisfy Koopmans' theorem.[35] These XC functionals are benchmarked against resolution-of-the-identity second-order coupled cluster (riCC2)[36] calculations. Furthermore, this work expands the

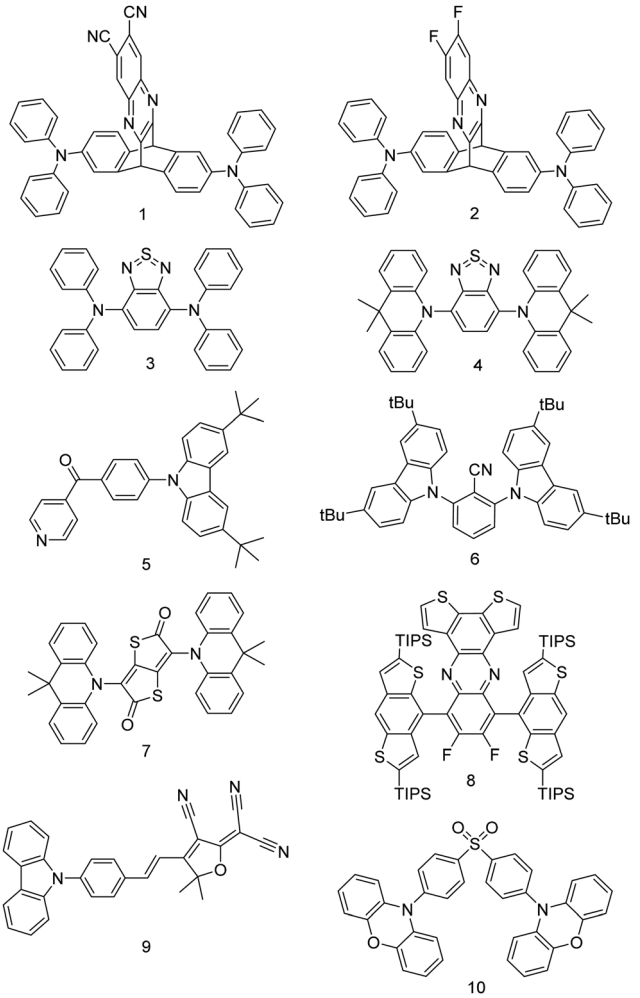

Fig. 1 Overview of the donor–acceptor compounds studied in this work.

investigation on the accurate determination of the singlet and triplet excitation energies beyond the first excited states. This could lead to useful insights in other fields outside that of TADF such as upper state photophysics,[37] singlet fission,[38] and photodynamic therapy (PDT).[39–41] Accurate determination of the second triplet excitation energy could be particularly useful for (image-guided) PDT applications[41–43] or when screening materials for their potential as efficient TADF emitters according to the vibronic mechanism, without going as far as calculating the spin–orbit coupling or vibronic interactions.

2 Materials and methods

2.1 Synthesis and optical characterizations

Compounds **1**,[9] **3–6**,[44–46] and **9**[47] were synthesized according to their respective literature procedures. Compound **10** was obtained from Lumtech Inc (LT-N545). Syntheses of **2**, **7**, and **8** were performed following the procedures presented in Scheme 1. TPA-DK[9] and 1,4-dibromo-2,3-difluoro-5,6-dinitrobenzene[48] were synthesized according to their respective literature procedures. Details with respect to the synthesis and characterization of these compounds are provided in the ESI.†

All electronic absorption spectra were measured on a Varian Cary 5000 UV-Vis-NIR spectrophotometer from Agilent Technologies. Corrected steady-state emission spectra were recorded on a Horiba-Jobin Yvon Fluorolog-3 spectrofluorometer equipped with a 450 W xenon lamp as light source, with excitation at the ascending slope of the charge transfer absorption band. Freshly prepared samples in 1 cm quartz cells were used to perform all UV-Vis-NIR absorption and fluorescence measurements. Fluorescence measurements were performed using 10 mm optical path length cuvettes under a right-angle arrangement. All spectroscopic measurements were done in non-degassed samples at 20 °C in spectroscopic grade toluene.

2.2 Theoretical and computational details

The ground-state geometries of all compounds were fully optimized at the M06/6-311G(d) level.[49] All vibrational frequencies are real, demonstrating the optimized geometries correspond to minima on the potential energy surface. For compound **8**, the triisopropysilyl (TIPS) groups were substituted by H atoms to reduce the computational cost. Adiabatic TD-DFT calculations were performed using a variety of XC functionals (Table 1), ranging from GGA, meta-GGA and global hybrid to range-separated hybrid XC functionals using the 6-311G(d) basis set. For the LC-BLYP and LC-ωPBE range-separated hybrids, the range-separating parameter ω was modified. The modified versions of LC-BLYP and LC-ωPBE are henceforth denoted with the respective value of ω in the name: LC-BLYP33 [which is a condensed notation for LC-BLYP(ω = 0.33)], LC-BLYP20, LC-BLYP17, and LC-ωPBE17. All excited state calculations were performed using the PCM model (cyclohexane) to account for an apolar environment. In addition to TD-DFT calculations, its Tamm–Dancoff approximation was also applied for all functionals and all compounds, allowing the assessment of its performance with respect to TD-DFT. From the excited state calculations, the vertical excitation energies to the S_1 ($\Delta E_{S_0\text{–}S_1} = E_{S_1} - E_{S_0}$), S_2 ($\Delta E_{S_2\text{–}S_0} = E_{S_2} - E_{S_0}$), T_1 ($\Delta E_{T_1\text{–}S_0} = E_{T_1} - E_{S_0}$) and T_2 ($\Delta E_{T_2\text{–}S_0} = E_{T_2} - E_{S_0}$) states, the oscillator strengths of the corresponding $S_0 \rightarrow S_1$ and $S_0 \rightarrow S_2$ transitions ($f_{S_0\text{–}S_1}$ and $f_{S_0\text{–}S_2}$), and the dominant one-electron transitions (molecular orbital pairs) for $S_0 \rightarrow S_1$ and $S_0 \rightarrow T_1$ transitions were obtained. From these values, $\Delta E_{S_1\text{–}T_1} = \Delta E_{S_1\text{–}S_0} - \Delta E_{T_1\text{–}S_0}$ (also referred to as ΔE_{ST}) and $\Delta E_{T_2\text{–}T_1} = \Delta E_{T_2\text{–}S_0} - \Delta E_{T_1\text{–}S_0}$ were calculated. All DFT and TD-DFT/TDA calculations were performed using the Gaussian09 program.[50]

The vertical excitation properties obtained with TD-DFT and TD-DFT/TDA were benchmarked using the resolution-of-the-identity approximation of the second-order approximated coupled-cluster model[36] using the Turbomole program (Version 7.3.1).[51] The resolution of the identity approximation for two-electron integrals reduces the CPU time needed to calculate these integrals. In addition, the method uses a partitioned form of the CC2 equations, eliminating the need to store double excitation cluster amplitudes. Using the riCC2 method allows computation of much larger systems such as the ones used in this work, whereas they would be difficult to perform with the unaltered CC2 method. Schreiber *et al.*[52] showed that the vertical excitation

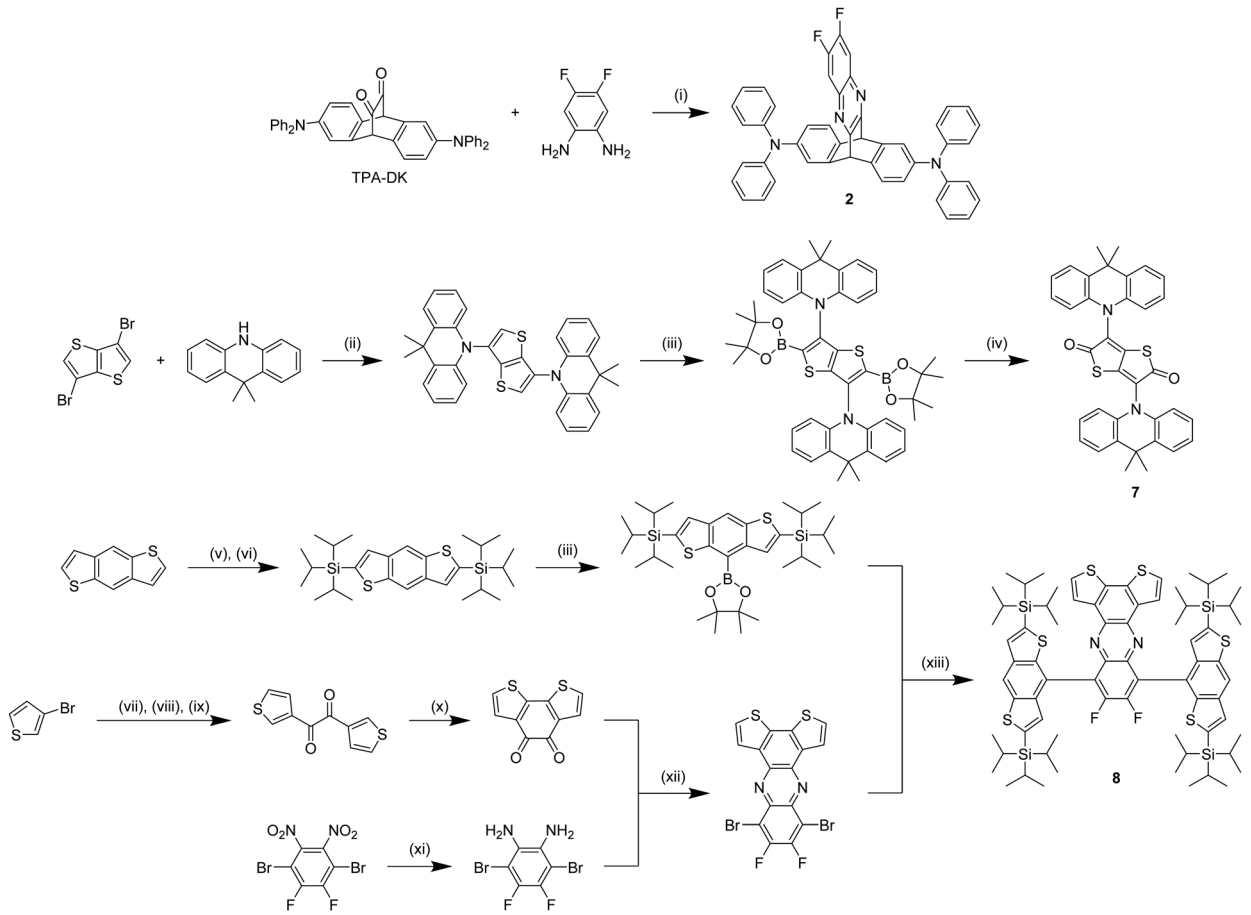

Scheme 1 Synthesis procedures for compounds **2**, **7**, and **8**: (i) ethanol/acetic acid (19/1) at reflux for 1 h; (ii) $Pd(OAc)_2$, XPhos and Na(O*t*Bu) in toluene at 110 °C for 24 h; (iii) bis(pinacolato)diboron, $[Ir(OMe)(COD)]_2$, 4,4′-di-*tert*-butyl-2,2′-bipyridine in dry cyclohexane at 80 °C for 24 h; (iv) Oxone™ in THF/H_2O (10/1) at room temperature for 3 h; (v) *n*-BuLi, dry THF at 0 °C for 1 h, (vi) TIPSCl, dry THF at 65 °C for 16 h; (vii) *n*-BuLi, dry THF at −78 °C for 1 h; (viii) CuBr, LiBr in dry THF at 0 °C for 1 h; (ix) oxalyl chloride at 0 °C for 1 h; (x) $FeCl_3$, CH_3NO_2 in CH_2Cl_2 at room temperature for 3 h; (xi) iron powder in acetic acid at 45 °C for 6 h; (xii) acetic acid at 75 °C for 16 h; (xiii) $Pd(PPh_3)_4$, K_2CO_3 in DMF/H_2O (4/1) at 130 °C for 24 h.

Table 1 Overview of the selected XC functionals grouped by their position on Jacob's ladder

	XC functional	% HF exchange[a]	Range-separating parameter ω[b] (Bohr^{-1})
GGA	BLYP		
	BPW91		
	PBE		
Meta-GGA	M06L		
	TPSS		
Global hybrid GGA	B3LYP	20	
	B971	21	
	PBE0	25	
Global hybrid meta-GGA	TPSSh	10	
	M06	27	
	M06-2X	54	
Long-range separated hybrid GGA/meta-GGA	ωB97	0–100	0.40 (1.323)
	ωB97X	16–100	0.30 (1.764)
	CAM-B3LYP	19–65	0.33 (1.604)
	LC-ωPBE17	0–100	0.17 (3.113)
	LC-BLYP17	0–100	0.17 (3.113)
	LC-BLYP20	0–100	0.20 (2.646)
	LC-BLYP33	0–100	0.33 (1.604)
	LC-BLYP	0–100	0.47 (1.126)

[a] For long-range corrected functionals, the % HF exchange is given at interelectronic distance $r_{12} = 0$ and ∞. [b] Corresponding length $L = 1/\omega$ (Å) in parentheses.

energies obtained with CC2 are in good agreement with those obtained with even higher levels of approximation such as the third-order approximation of the coupled cluster (CC3) and coupled cluster singles, doubles and triples (CCSDT) when the excitations exhibit a single excitation nature. Indeed, in these benchmarks on small- and medium-size closed-shell organic molecules, for singlet excitation energies, the mean absolute errors (MAEs) with respect to the CASPT2 reference data amount to 0.32 eV, 0.50 eV, and 0.22 eV for the CC2, CCSD, and CC3 methods, whereas for the triplet excitation energies, the MAEs given in the same order are 0.19 eV, 0.16 eV, and 0.08 eV, respectively. An alternative choice for the benchmark calculations might have been the spin-scaled-component version of CC2, SCS-CC2,[53] but recent investigations on the prediction of the valence excitation energies of closed-shell organic chromophores did not demonstrate an advantage for employing or not the spin-scaled-component scheme.[29,53–55] The same ground-state geometries were used for the riCC2 calculations as for the TD-DFT and TD-DFT/TDA calculations to exclude any geometry dependent differences. For these Turbomole calculations, def2-TZVP was chosen both as the main and auxiliary basis set as it also comprises split-valence triple zeta basis functions with polarization functions for the second- and third-row atoms. Additional TD-DFT/def2-TZVP calculations were performed to demonstrate that the use of different basis sets for the riCC2 and TD-DFT calculations has a negligible impact. Indeed, at the TD-DFT/LC-BLYP17 level, differences of excitation energies between the def2-TZVP and 6-311G* basis sets are always smaller than 0.08 eV and the mean absolute difference amounts to 0.03 eV. Moreover, the impact of the ground state geometries on the first singlet and triplet excitation energies has been assessed by performing additional TD-DFT/LC-BLYP17 excitation energy calculations on geometries optimized at the ωB97X-D/6-311G(d) level of approximation. The ωB97X-D[56] XC functional accounts explicitly for London dispersion forces by using empirical expressions, whereas M06 was parameterized to account, implicitly, for London dispersion interactions. The differences of TD-DFT/LC-BLYP17 excitation energies between the M06 and ωB97X-D optimized geometries is negligible, with a mean absolute difference of 0.04 eV.

The mean absolute errors (MAEs), mean signed errors (MSEs), and standard deviations are calculated for all XCFs and for both TD-DFT and TD-DFT/TDA schemes in comparison to the reference riCC2 results (difference = TD-DFT − riCC2). The absolute average errors help to objectively determine the most accurate XC functional, whereas the sign-dependent average errors yield some insight to whether the chosen XC functional tends to over- or underestimate the given property.

3 Results and discussion

3.1 Experimental spectroscopic results and earlier theoretical data

Results from the literature are summarized in Table 2 for the electronic and optical properties of compounds **1**, **3–6**, and **9–10**. These include experimental data as well as TD-DFT results related to the first singlet and triplet excited states. Our experimental UV-Vis absorption and emission data are also given for the whole list of compounds. Compound **7** was found to be non-emissive. Although the differences between literature results and ours are generally small (a few tenths of eV), the ΔE_{max} of absorption of **9** differs by more than one eV. As discussed below, the new value is much more consistent with the quantum-chemical calculations. This new experimental value of **9** substantiates the fact that we enacted our own set of optical characterizations.

3.2 Reference riCC2 calculations

The benchmark riCC2 values used to reference the TD-DFT and TD-DFT/TDA calculations are given in Table 3. The agreement between the first vertical singlet excitation energies ($\Delta E_{S_0-S_1}$) calculated using riCC2 and the experimental absorption maxima was verified by constructing a correlation plot between the two properties (Fig. 2). The slope of the correlation plot is slightly larger than 1, indicating that the riCC2 vertical excitation energy increases more rapidly with increasing absorption maximum. The R^2 value of 0.95 points to a very good correlation between the two properties, proving the high level of predictability of riCC2 calculations in comparison to experimental

Table 2 Experimental and theoretical properties of the selected compounds

	ΔE_{max}, eV (λ_{max}, nm) abs.[a]	ΔE_{max}, eV (λ_{max}, nm) em.[a]	ΔE_{max}, eV (λ_{max}, nm) abs.[b]	ΔE_{max}, eV (λ_{max}, nm) em.[b]	$\Delta E_{T_1-S_0}$[d], eV	ΔE_{ST}[d], eV	Calc. $\Delta E_{T_1-S_0}$[e], eV	XC functional and basis set[e]
1[9]	2.95 (420)	2.25 (552)	2.95 (421)	2.15 (578)	—	—	0.11	B3LYP/6-31G(d)
2	—	—	3.37 (368)	2.55 (486)	—	—	—	—
3[45]	2.43 (510)	1.91 (648)	2.43 (510)	1.86 (668)	—	—	0.69	LC-ωPBE/6-31G(d)[f]
4[45]	2.57 (482)	1.94 (638)	2.58 (481)	1.92 (645)	2.12	0.11	0.02	LC-ωPBE/6-31G(d)[f]
5[46]	3.32 (373)	2.65 (467)	3.31 (375)	2.62 (473)	2.84	0.13	0.32	B3LYP/6-31G
6[44]	3.38 (367)	2.99 (414)	3.43 (362)	2.99 (414)	2.97	0.26	0.13	B3LYP/6-31G(d,p)
7	—	—	2.02 (613)	—[c]	—	—	—	—
8	—	—	2.88 (430)	2.24 (553)	—	—	—	—
9[47]	3.67 (338)	2.10 (590)	2.58 (480)	2.06 (602)	1.95	0.10	0.68	B3LYP/6-31G(d)
10[57]	~3.18 (~390)	2.45 (507)	3.14 (395)	2.39 (519)	2.65	0.08	0.03	B3LYP/6-31G(d)

[a] Experimental ΔE_{max} (λ_{max}) for the absorption ($S_0 \rightarrow S_1$) and emission ($S_1 \rightarrow S_0$) in toluene as taken from the respective references. [b] Experimental ΔE_{max} (λ_{max}) for the absorption ($S_0 \rightarrow S_1$) and emission ($S_1 \rightarrow S_0$) in toluene as measured in this work. [c] No fluorescence observed. [d] Experimental values obtained from the corresponding literature. [e] TD-DFT values taken from the respective references. [f] The authors make no reference to modification of the range-separating parameter, which is therefore expected to be default (ω = 0.33).

Table 3 riCC2 excitation energies, oscillator strengths, and energy gaps for compounds **1–10**

	$\Delta E_{S_0-S_1}$ (eV)	$\Delta E_{S_0-S_2}$ (eV)	$f_{S_0-S_1}$	$f_{S_0-S_2}$	$\Delta E_{S_0-T_1}$ (eV)	$\Delta E_{S_0-T_2}$ (eV)	$\Delta E_{T_1-T_2}$ (eV)	$\Delta E_{S_1-T_1}$ (eV)
1	2.969	2.996	0.170	0.098	2.903	2.948	0.045	0.067
2	3.468	3.496	0.157	0.131	3.337	3.354	0.016	0.130
3	2.474	3.355	0.231	0.008	2.081	3.256	1.175	0.393
4	2.456	2.525	0.000	0.000	2.457	2.527	0.069	−0.001
5	3.524	3.718	0.396	0.004	3.227	3.411	0.185	0.297
6	3.565	3.646	0.207	0.001	3.494	3.502	0.009	0.071
7	1.923	1.882	0.094	0.002	1.852	1.853	0.001	0.029
8	3.076	3.150	0.083	0.005	2.575	2.961	0.386	0.501
9	2.692	3.488	1.011	0.585	2.159	2.809	0.651	0.534
10	3.022	3.031	0.032	0.010	3.010	3.019	0.009	0.012

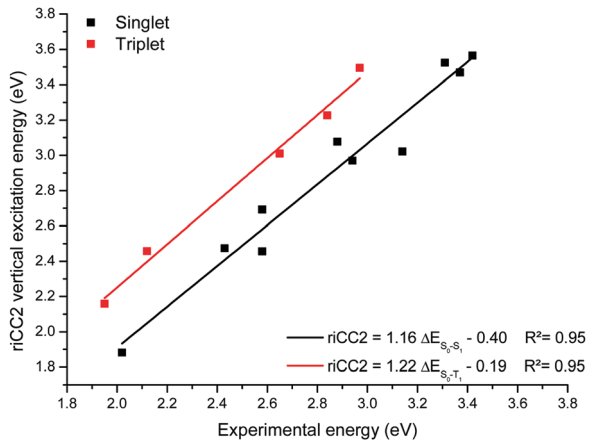

Fig. 2 Correlation plots between the riCC2 vertical excitation energies and the experimental values for maximum absorption $\Delta E_{S_0-S_1}$ and $\Delta E_{S_0-T_1}$.

values. Although the number of points is reduced, a similarly good correlation between riCC2 and experiment is observed for the $S_0 \rightarrow T_1$ transition energies. For ΔE_{ST} no valid correlation could be drawn, probably because the experimental values are not obtained from the difference between $\Delta E_{S_0-S_1}$ and $\Delta E_{S_0-T_1}$, but rather from the onsets of the fluorescence (at room temperature) and phosphorescence (at 77 K) CT emission peaks.

3.3 TD-DFT and TD-DFT/TDA *versus* riCC2 calculations

Singlet excitation energies and oscillator strengths. For the vertical singlet excitation energies and the corresponding oscillator strengths, the choice was made to only consider states that have the same nature in both the riCC2 and the TD-DFT or TD-DFT/TDA calculations. With the exception of compound **7** (HOMO−1 → LUMO), the dominant nature of the first excited state of all compounds is of HOMO → LUMO character for the riCC2 calculations. Given the near degeneracy (Table 3) of the first and second vertical excitation energies, and to have the comparison between the compounds more in line with each other, we have chosen to take the HOMO → LUMO transition as the first state and the HOMO−1 → LUMO transition as the second state for compound **7**. In a few compound-functional combinations, the nature of the first singlet excited state calculated with TD-DFT or TD-DFT/TDA does not correspond to a HOMO → LUMO transition. We then opted to use the second (HOMO → LUMO) excited state to compare states of the same nature. Indeed, comparison between two states of different nature may lead to faulty conclusions about the XCFs ability to correctly predict the targeted properties. These statistical analyses are provided in Table 4 for TD-DFT values and in Table 5 for the TD-DFT/TDA ones. The full list of all compounds and their excited state data for the first two states can be found in the ESI.†

In Fig. 3, each colored line represents a single XCF and the sign-dependent error with respect to the riCC2 calculation is plotted for every compound. For the first singlet excitation

Table 4 Statistical analysis including mean absolute errors (MAEs, eV) and standard deviations (eV) obtained from the comparison between TD-DFT calculations with different XCFs and riCC2 reference values

	$\Delta E_{S_0-S_1}$ (eV)		$f_{S_0-S_1}$		$\Delta E_{S_0-S_2}$ (eV)		$f_{S_0-S_2}$		$\Delta E_{S_0-T_1}$ (eV)		$\Delta E_{S_0-T_2}$ (eV)		ΔE_{T_1-T2} (eV)		$\Delta E_{S_1-T_1}$ (eV)	
	MAE	StdDev	MAE	StdDev	MAE	StdDev	MAE	StdDev	MAE	StdDev	MAE	StdDev	MAE	StdDev	MAE	StdDev
BLYP	1.242	0.213	0.116	0.144	1.329	0.231	0.072	0.173	1.153	0.265	1.224	0.190	0.139	0.161	0.113	0.144
BPW91	1.236	0.216	0.113	0.143	1.322	0.230	0.072	0.173	1.153	0.266	1.220	0.193	0.138	0.160	0.111	0.142
PBE	1.238	0.216	0.113	0.143	1.322	0.229	0.072	0.173	1.153	0.268	1.225	0.195	0.144	0.168	0.112	0.142
M06L	1.021	0.202	0.109	0.138	1.102	0.237	0.072	0.173	0.952	0.224	1.005	0.178	0.130	0.145	0.100	0.130
TPSS	1.166	0.204	0.110	0.139	1.244	0.223	0.069	0.173	1.090	0.251	1.151	0.188	0.137	0.155	0.105	0.138
TPSSh	0.850	0.149	0.095	0.119	0.904	0.191	0.072	0.173	0.820	0.158	0.845	0.157	0.115	0.137	0.078	0.083
B3LYP	0.596	0.110	0.074	0.089	0.628	0.172	0.070	0.173	0.610	0.086	0.605	0.112	0.076	0.090	0.054	0.048
B971	0.555	0.102	0.068	0.083	0.583	0.169	0.070	0.173	0.566	0.083	0.563	0.105	0.072	0.084	0.053	0.046
PBE0	0.430	0.089	0.053	0.064	0.445	0.164	0.119	0.229	0.526	0.068	0.482	0.080	0.049	0.059	0.096	0.070
M06	0.379	0.106	0.050	0.057	0.399	0.179	0.068	0.173	0.460	0.089	0.430	0.091	0.035	0.037	0.081	0.068
M06-2X	0.283	0.102	0.084	0.107	0.257	0.109	0.024	0.050	0.162	0.081	0.133	0.095	0.081	0.081	0.239	0.112
ωB97	0.882	0.239	0.254	0.233	0.850	0.238	0.088	0.150	0.388	0.196	0.351	0.243	0.362	0.311	1.263	0.161
ωB97X	0.740	0.215	0.225	0.224	0.713	0.203	0.060	0.135	0.311	0.184	0.300	0.221	0.332	0.287	1.044	0.142
CAM-B3LYP	0.311	0.124	0.101	0.145	0.316	0.118	0.047	0.084	0.332	0.177	0.234	0.133	0.213	0.162	0.643	0.119
LC-ωPBE17	0.141	0.102	0.051	0.101	0.182	0.086	0.048	0.117	0.344	0.099	0.302	0.086	0.050	0.057	0.209	0.127
LC-BLYP17	0.157	0.106	0.050	0.098	0.192	0.085	0.042	0.115	0.314	0.089	0.287	0.079	0.039	0.042	0.156	0.102
LC-BLYP20	0.107	0.074	0.086	0.138	0.075	0.074	0.052	0.128	0.215	0.129	0.157	0.076	0.072	0.072	0.270	0.136
LC-BLYP33	0.650	0.192	0.210	0.211	0.600	0.195	0.058	0.137	0.231	0.161	0.248	0.179	0.245	0.220	0.868	0.125
LC-BLYP	0.978	0.264	0.270	0.236	0.956	0.262	0.117	0.204	0.623	0.239	0.492	0.248	0.400	0.354	1.601	0.187
LC-BLYP20-M06-2X	—	—	—	—	—	—	—	—	—	—	—	—	—	—	0.155	0.090

Table 5 Statistical analysis including mean absolute errors (MAEs, eV) and standard deviations (eV) obtained from the comparison between TD-DFT/TDA calculations with different XCFs and riCC2 reference values

	$\Delta E_{S_0-S_1}$ (eV)		$f_{S_0-S_1}$		$\Delta E_{S_0-S_2}$ (eV)		$f_{S_0-S_2}$		$\Delta E_{S_0-T_1}$ (eV)		$\Delta E_{S_0-T_2}$ (eV)		$\Delta E_{T_1-T_2}$ (eV)		$\Delta E_{S_1-T_1}$ (eV)	
	MAE	StdDev	MAE	StdDev	MAE	StdDev	MAE	StdDev	MAE	StdDev	MAE	StdDev	MAE	StdDev	MAE	StdDev
BLYP	1.220	0.226	0.098	0.118	1.318	0.242	0.071	0.173	1.148	0.269	1.222	0.191	0.142	0.165	0.112	0.137
BPW91	1.214	0.229	0.096	0.117	1.310	0.242	0.071	0.173	1.146	0.272	1.217	0.194	0.141	0.164	0.111	0.136
PBE	1.215	0.229	0.096	0.116	1.311	0.241	0.071	0.173	1.147	0.273	1.218	0.196	0.142	0.165	0.112	0.136
M06L	1.001	0.213	0.093	0.117	1.092	0.245	0.072	0.173	0.932	0.240	0.992	0.184	0.135	0.153	0.105	0.136
TPSS	1.144	0.216	0.094	0.114	1.236	0.236	0.071	0.173	1.079	0.259	1.143	0.193	0.138	0.160	0.108	0.135
TPSSh	0.828	0.160	0.076	0.097	0.894	0.198	0.070	0.173	0.784	0.190	0.818	0.171	0.129	0.151	0.094	0.116
B3LYP	0.574	0.120	0.055	0.071	0.618	0.177	0.069	0.173	0.560	0.122	0.580	0.122	0.102	0.108	0.074	0.081
B971	0.533	0.113	0.050	0.065	0.573	0.173	0.068	0.173	0.520	0.116	0.540	0.115	0.097	0.101	0.072	0.077
PBE0	0.407	0.099	0.036	0.047	0.435	0.168	0.067	0.173	0.436	0.079	0.444	0.082	0.068	0.064	0.064	0.056
M06	0.356	0.113	0.035	0.045	0.389	0.182	0.067	0.173	0.372	0.079	0.371	0.113	0.080	0.083	0.061	0.062
M06-2X	0.322	0.088	0.100	0.137	0.289	0.116	0.017	0.026	0.144	0.127	0.177	0.101	0.052	0.045	0.187	0.104
ωB97	0.966	0.208	0.287	0.274	0.903	0.234	0.051	0.118	0.236	0.183	0.385	0.269	0.155	0.172	0.731	0.103
ωB97X	0.812	0.187	0.255	0.265	0.758	0.199	0.047	0.114	0.210	0.166	0.322	0.213	0.129	0.135	0.612	0.100
CAM-B3LYP	0.356	0.105	0.119	0.171	0.351	0.109	0.037	0.047	0.151	0.090	0.127	0.103	0.067	0.074	0.303	0.127
LC-ωPBE17	0.128	0.087	0.065	0.125	0.153	0.089	0.064	0.120	0.273	0.078	0.264	0.089	0.043	0.038	0.171	0.109
LC-BLYP17	0.141	0.092	0.066	0.123	0.164	0.090	0.026	0.069	0.262	0.075	0.261	0.079	0.036	0.021	0.137	0.090
LC-BLYP20	0.118	0.097	0.107	0.171	0.088	0.072	0.036	0.088	0.149	0.066	0.123	0.052	0.044	0.040	0.226	0.130
LC-BLYP33	0.721	0.168	0.241	0.254	0.645	0.194	0.047	0.113	0.175	0.149	0.255	0.184	0.100	0.098	0.563	0.127
LC-BLYP	1.073	0.230	0.305	0.280	1.030	0.254	0.061	0.119	0.199	0.181	0.351	0.307	0.171	0.186	0.883	0.125
LC-BLYP20-M06-2X	—	—	—	—	—	—	—	—	—	—	—	—	—	—	0.146	0.097

energy (Fig. 3a), we can clearly see some functionals heavily overestimating (LC-BLYP, ωB97, ωB97X, LC-BLYP33) and some functionals underestimating (PBE, BPW91, BLYP, TPSS, M06L, TPSSh, B3LYP, B971, PBE0, M06) the singlet excitation energy. Overestimation of the singlet excitation energy typically occurs when there is too much HF exchange, *i.e.*, for range-separated hybrids when the range-separating parameter is not properly tuned (ω is too large). Underestimation happens when there is not enough HF exchange present, as is the case for the GGA and meta-GGA functionals, but even for some of the hybrid functionals. This originates from the ultra-locality of the XCF and the related self-interaction error, leading to a poor description of the CT excitations.[58,59] We also observe some variations of the errors as a function of the nature of the compounds, but most XC functionals seem to follow the same trend. The absolute values of the errors depicted in Fig. 3 are averaged per functional in Table 4 and are provided together with their standard deviation. From Table 4, the functionals that show a relatively small error are CAM-B3LYP (0.311 eV) and M06-2X (0.283 eV), but they are outperformed by LC-ωPBE17 (0.141 eV), LC-BLYP17 (0.157 eV) and LC-BLYP20 (0.141 eV). From the difference between the signed and absolute errors (Table S1, ESI†), it is also clear that LC-BLYP20 tends to either slightly over- or underestimate the singlet excitation energy for a given compound. This is likely due to the small size of the error, as the other functionals all show the same amplitudes for the signed and absolute errors. Taking the LC-BLYP XCFs, the signed errors range from −0.157 eV (ω = 0.17, the amount of HF exchanges grows the least rapidly with r_{12}) to 0.056 eV (ω = 0.20), 0.650 eV (ω = 0.33), and 0.978 eV (ω = 0.47, the amount of HF exchanges grows the fastest with r_{12}), demonstrating the key role of long-range exchange. Using the Tamm–Dancoff approximation has a minor impact in the sense that large underestimations or overestimations of $\Delta E_{S_0-S_1}$ remain when employing that approximation.

The second vertical singlet energy, $\Delta E_{S_0-S_2}$, follows the same trend as the first vertical singlet energy. A decrease in the MAE is observed with increasing HF exchange until a minimum is reached and the error increases again as the amount of HF exchange becomes too high. The most notable XC functionals are the same as for the first vertical singlet energy, LC-ωPBE17 (0.182 eV), LC-BLYP17 (0.192 eV) and LC-BLYP20 (0.182 eV). Again, there is little difference between the TD-DFT and TD-DFT/TDA results. For both singlet excitation energies, LC-BLYP20 gives the smallest MAEs. The standard deviations on the MAEs for both properties are related to the MAEs themselves. If the MAE decreases, so does the standard deviation and *vice versa*. A slight exception to this is M06-2X (0.102 eV), which has relatively small standard deviations, still comparable to LC-BLYP17 (0.106 eV) and LC-ωPBE17 (0.102 eV), despite having a MAE that is nearly twice as large.

For the oscillator strengths, the analysis is less straightforward because their amplitudes cover more than one order of magnitude [even after neglecting those states with very small ($f < 0.05$) values]. Moreover, as shown in Table 3 (riCC2 values), with exception of compound **9**, all compounds show relatively small to very small oscillator strengths. This is most definitely true for the oscillator strength of the $S_0 \rightarrow S_2$ transition. As a matter of fact, for these very small oscillator strengths, most XCFs perform well because they reproduce the dominant character of the transition, which determines the negligible *f* values. This is illustrated by compound **4**, where the $S_0 \rightarrow S_1$ and $S_0 \rightarrow S_2$ transitions have a CT character, between the donor and acceptor groups that are perpendicular to each other (and therefore of different symmetry). To a given extent, the same trend as for the first singlet excitation energies roughly holds. This is expected as a good representation of the excitation energy should give a good description of its oscillator strength. Then, as already observed for benzene

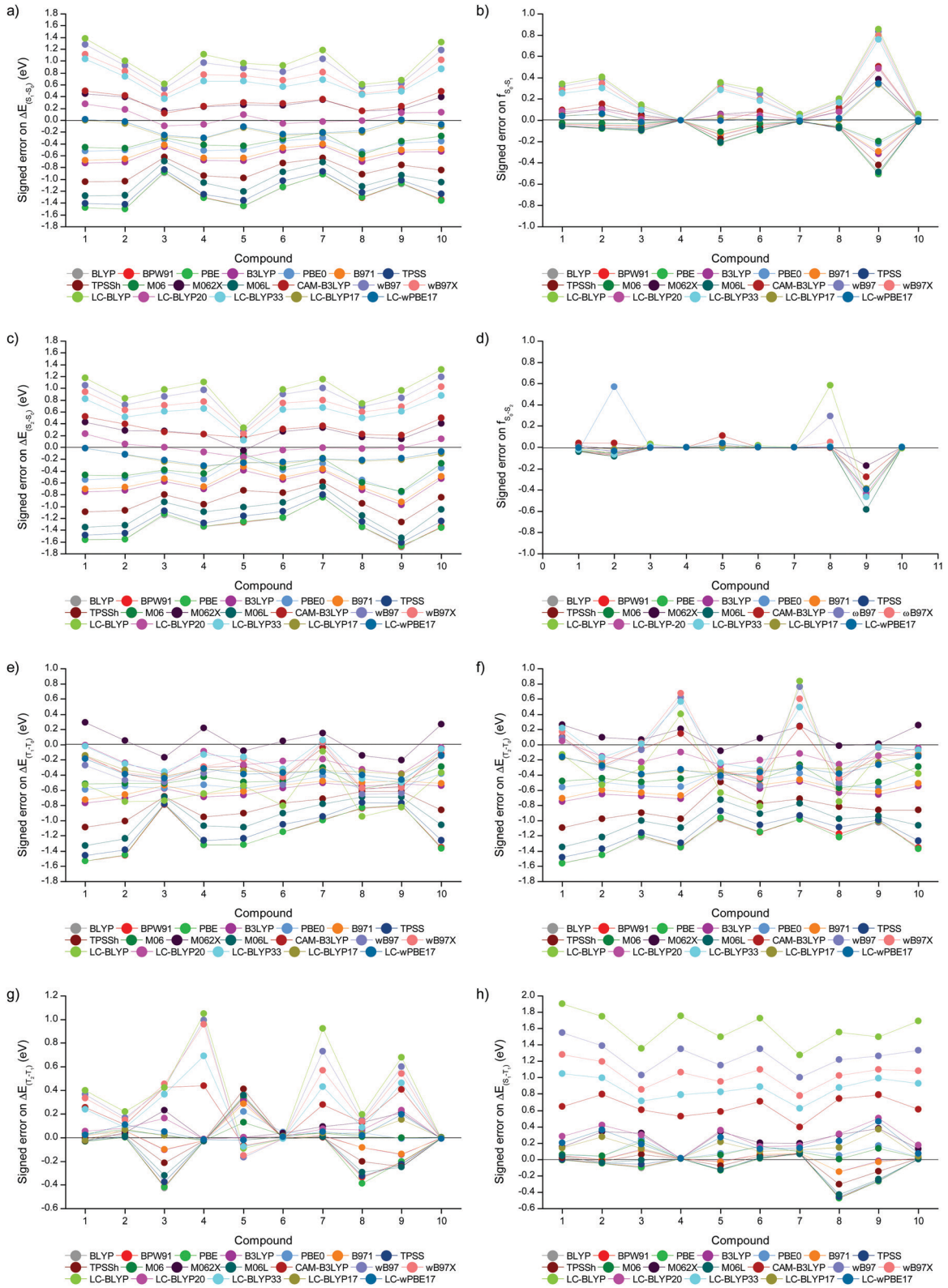

Fig. 3 Signed errors on each property for each individual XC functional for all 10 compounds obtained using TD-DFT. (a) First vertical singlet excitation energy, $\Delta E_{S_0-S_1}$. (b) Oscillator strength for the first singlet excitation, $f_{S_0-S_1}$. (c) Second vertical singlet excitation energy, $\Delta E_{S_2-S_0}$. (d) Oscillator strength for the second vertical singlet excitation, $f_{S_0-S_2}$. (e) First vertical triplet excitation energy, $\Delta E_{T_1-S_0}$. (f) Second vertical triplet excitation energy, $\Delta E_{T_2-S_0}$. (g) Triplet–triplet energy gap for the first two triplet excited states, $\Delta E_{T_2-T_1}$. (h) Singlet–triplet gap for the first singlet and triplet excited states, $\Delta E_{S_1-T_1}$.

derivatives, XCFs with a small amount of HF exchange underestimate both the excitation energies and oscillator strengths.[60] For the $S_0 \rightarrow S_1$ transition, a large number of functionals are within 0.2 of each other and give relatively consistent results. Functionals such as LC-BLYP17 (0.050 eV), LC-ωPBE17 (0.051 eV), LC-BLYP20 (0.086 eV), M06-2X (0.084 eV), CAM-B3LYP (0.101 eV), M06 (0.050 eV), PBE0 (0.053 eV), B971 (0.068 eV), B3LYP (0.074 eV) and TPSSh (0.095 eV) all have errors below 0.1, albeit their standard deviations are larger than the errors themselves (since the errors originate from a few excited states only). Using the Tamm–Dancoff approximation again barely changes these general conclusions, although, in more detail, its impact depends on the XCF and on the excited state (S_1 or S_2). Indeed, the absolute average error decreases slightly for most functionals, except for M06-2X and the range-separated functionals when looking at the $S_0 \rightarrow S_1$ transition. For the $S_0 \rightarrow S_2$ transition, the MAEs decrease slightly for all functionals except for LC-ωPBE17 and LC-BLYP. The best performing functionals for both transitions are M06-2X, LC-BLYP17, LC-ωPBE17, and LC-BLYP20.

First and second triplet excitation energies. To achieve efficient intersystem crossing, the ^{3}CT and ^{3}LE state (or ^{3}CT state of a different nature) need to be close in energy for efficient vibronic coupling to take place. Therefore, this work not only focuses on calculating the first, but also the second vertical triplet excitation energies (Fig. 3 and Tables 4, 5). Looking at the data obtained using the TD-DFT approach, the error on the first triplet excitation energy, $\Delta E_{S_0-T_1}$, is the smallest for M06-2X (0.162 eV). This is consistent with the results of Brückner *et al.*[9a] in their report on the singlet–triplet gap for triplet–triplet annihilation. When looking at the other functionals that perform well, LC-BLYP20 (0.215 eV), LC-BLYP33 (0.231 eV), ωB97X (0.311 eV), LC-BLYP17 (0.314 eV), CAM-B3LYP (0.332 eV), and LC-ωPBE17 (0.344 eV) all have absolute average errors within 0.35 eV. It is apparent that a substantially high amount of HF exchange is necessary to accurately describe the triplet energy as is observed for the LC-BLYP functionals with ω = 0.20 and 0.33 which outperform those with ω = 0.17 and LC-ωPBE17. On the other hand, the unmodified LC-BLYP has a much higher MAE, indicating a too large value for ω. The MAEs for the second vertical triplet excitation energy, $\Delta E_{S_0-T_2}$, follow the same trend as for the first excitation energy and are even a bit smaller for all functionals.

When comparing TD-DFT with TD-DFT/TDA, all functionals show a more consistent behavior throughout the series (Fig. S1, ESI†). The accuracy of all functionals increases as can be seen by a decrease of the absolute average error for all functionals. Most notable are CAM-B3LYP (0.332 eV $\rightarrow$ 0.151 eV) and LC-BLYP (0.623 eV $\rightarrow$ 0.199 eV), which gain significant accuracy and have smaller standard deviations when using the TD-DFT/TDA approach. Upon using the TDA, a number of functionals, comprising M06-2X (0.144 eV), CAM-B3LYP (0.151 eV), LC-BLYP20 (0.149 eV), LC-BLYP33 (0.175 eV), and LC-BLYP (0.199 eV), have absolute average errors within 200 meV. The sudden decrease in MAE for the vertical triplet excitation energies using functionals such as CAM-B3LYP and LC-BLYP is attributed to the ground state triplet instability problem for these systems, which is known to occur when using XCFs with a large amount of HF exchange.[58,59,61,62] In the TDA, only excitation between occupied-virtual orbital pairs is allowed as opposed to conventional TD-DFT, where virtual-occupied de-excitation contributions are also allowed. The form of the TDA eigenvalue equation precludes the occurrence of imaginary excitation energies and hence circumvents the triplet instability issues that can arise. Still, the triplet instability problem has smaller impact for our set of selected compounds than in the case of cyanines.[59,62]

The error on the second triplet excitation energy is the smallest for M06-2X (0.133 eV) and furthermore it has also the smallest standard deviation. Second best is LC-BLYP20 (0.157 eV), which, despite its relatively poor accuracy with respect to M06-2X, has a similar standard deviation and is closely followed by CAM-B3LYP (0.234 eV). Other functionals that are noteworthy are LC-ωPBE (0.302 eV), LC-BLYP17 (0.287 eV), and LC-BLYP33 (0.248 eV), all having absolute average errors within 0.3 eV. The overall performance is enhanced when using the TDA, except for M06-2X, in which the absolute average error goes up by 25% (0.133 $\rightarrow$ 0.177 eV). Using TDA, LC-BLYP20 (0.123 eV) and CAM-B3LYP (0.127 eV) perform similarly.

Due to the vibronic enhancement, the T_1–T_2 energy gap can help to explain a compound's potential for TADF (Fig. 3 and Tables 4 and 5). The largest absolute average error is 0.400 eV (LC-BLYP), meaning that the errors are generally smaller than when looking at the energies of the individual states. This leads us to conclude that a large number of functionals benefit from a cancellation of two relatively large errors. Therefore, the discussion will mainly focus on the functionals that did well in estimating the transition energies to T_1 and T_2. The best performing functional is LC-BLYP17 (0.039 eV), followed by LC-ωPBE17 (0.050 eV), LC-BLYP20 (0.072 eV), and M06-2X (0.081 eV). Applying the Tamm–Dancoff approximation, the absolute average errors have significantly decreased further for the aforementioned functionals. Furthermore, CAM-B3LYP (0.213 $\rightarrow$ 0.067 eV) performs a whole lot better under the TDA, as was also shown for the T_1 and T_2 energies.

Singlet–triplet energy gap. The first property that is typically considered when analyzing a compound for TADF, is the singlet–triplet energy gap. Its amplitude is correlated, with good approximation, to the spatial overlap between the HOMO and LUMO because the first singlet and triplet transitions are dominated by the HOMO-to-LUMO configuration. This is evidenced in Fig. S2 (ESI†) at the representative M06/6-311G(d) level of approximation. One would expect that the XC functionals that are accurately describing both the singlet and triplet excitation energies also perform well at describing the energy gap between them. Therefore, from the previous sections, it follows that LC-ωPBE17 (0.209 eV), LC-BLYP17 (0.156 eV), LC-BLYP20 (0.270 eV) and M06-2X (0.239 eV) are reliable functionals to use under the regular TD-DFT formalism, despite not having the smallest absolute errors or standard deviations. Ideally, TD-DFT/TDA is used and the error

on the energy gaps for LC-ωPBE17 (0.171 eV), LC-BLYP17 (0.137 eV), LC-BLYP20 (0.226 eV), and M06-2X (0.187 eV) is reduced. CAM-B3LYP (0.643 → 0.303 eV) still shows a relatively large error on ΔE_{ST} due to its larger average error on the singlet excitation energy than the other two functionals.

Surprisingly, most functionals, including the GGA and meta-GGA functionals without HF exchange (BLYP, BPW91, PBE, TPSS, M06L), perform well for the singlet–triplet energy gap. These data also explain why one of the most used functionals in literature (B3LYP), has not been found to give erroneous results, despite its poor ability to describe both the singlet and triplet excitation energies. The same goes for the other functionals. When looking at the singlet and triplet energies individually, they fail dramatically in predicting accurate values. The corresponding underestimations of both types of excitation energies have the same origin, which is related to the CT character of the excitations.[58] Therefore, their ability to accurately predict ΔE_{ST} is due to the compensation of two large errors, as was also seen for the T_1–T_2 energy gap. Ultimately, since they are obtained with the wrong underlying quantities, these functionals are not recommended, even though they might give a quantitatively correct answer for a certain set of compounds. Because of the large errors on the singlet and triplet excitation energies when using these functionals, one can never be sure that the calculated singlet–triplet energy gap is trustworthy, nor whether related quantities like the spin–orbit couplings could be accurate since they depend on the nature of the excited state.

Lastly, the possibility to use a 'hybrid' approach in which the vertical singlet and triplet excitation energies are calculated using two different functionals can be taken into consideration, *i.e.*, (i) LC-BLYP20 that gives the best results for the singlet excitation energies and (ii) M06-2X that provides the best results for the triplet excitation energies. Combining the results from both functionals shows mean absolute errors on the singlet–triplet energy gap of 0.155 eV using TD-DFT and 0.146 eV using TD-DFT/TDA (Tables 4 and 5). These values are comparable to those obtained with single functional calculations such as LC-BLYP17, but give better performance than functionals such as M06-2X and LC-BLYP20 separately.

Further discussion on the performance of the TD-DFT scheme with respect to riCC2. To further evaluate the XC functionals used in this work, the consistency of the TD-DFT and TD-DFT/TDA results *versus* the results obtained using riCC2 for the first excited singlet and triplet states was checked by constructing correlation plots. In Fig. 4, the correlation is given for LC-BLYP20, which is the best performing functional for the vertical singlet excitation energies and also performs well for the triplet vertical excitation energies. In Fig. S3 (ESI†), the correlation plots for all functionals used in this work can be found. While each of the functionals shows a linear correlation, the slopes vary widely from 0.66 to 1.07, with R^2 values varying from 0.73 to 0.98. XC functionals without HF exchange (BLYP, BPW91, PBE, M06L, and TPSS) reproduce the riCC2 values poorly, with slopes much smaller than 1 and R^2 values below 0.85. The group of functionals with a small percentage of

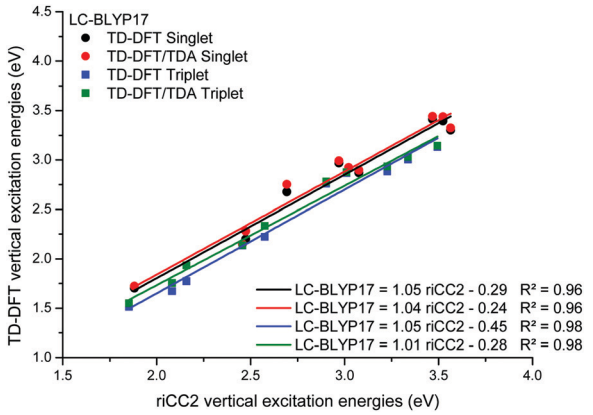

Fig. 4 Correlation between the LC-BLYP17 and riCC2 calculations for the first vertical singlet and triplet excitations.

HF exchange (TPSSh, B3LYP, B971, PBE0, M06, and M062X) performs significantly better, especially with increasing amount of HF exchange. Apart from TPSSh (with only 10% of HF exchange), these functionals are showing correlations with R^2 values above 0.95, but with slopes that are still only around 0.9. As the amount of HF exchange increases to 54% for M06-2X, slopes of around 1.0 with R^2 values of around 0.95 are found. Finally, the group of range-separated functionals (ωB97, ωB97X, CAM-B3LYP, LC-ωPBE17, LC-BLYP17, LC-BLYP20, LC-BLYP33, and LC-BLYP) shows varying behavior, depending on their range-separated parameter. Due to the, generally, higher amount of HF exchange, the slopes of the correlation plots are all in the range of 0.95–1.07, but the R^2 values change heavily. In the cases where the range-separating parameter is too large, the amount of HF exchange increases rapidly and the R^2 values get smaller, as is the case for ωB97, ωB97X, CAM-B3LYP, LC-BLYP33, and LC-BLYP. For the tuned range-separating functionals such as LC-ωPBE17, LC-BLYP17, and LC-BLYP20, both the slopes and R^2 values obtained are close to 1.0. Utilizing the Tamm–Dancoff approximation shows little influence on the correlation of the vertical singlet excitation energies, as was also shown above. For the correlation on the triplet excitation energies, the TD-DFT/TDA approach leads to a slight decrease in the slope and R^2 values for the hybrid and non-hybrid functionals and leads to a slight increase or decrease in the slope depending on whether the slope was smaller or larger than 1.0 and a slight increase in the R^2 values for the range-separated functionals. Overall, it means the TDA approach gives a better correlation (closer to 1) for the range-separated functionals with an increased R^2. It is further interesting to analyze the intercepts at the origin for the different first singlet and triplet excitation energies, which are directly related to a comparison of the regression lines. For GGA, mGGA, and hybrids with small amount of HF exchange, these intercepts vary little from the singlet to triplet excitation energies or from the TD-DFT to the TD-DFT/TDA calculations (typically by less than 0.2 eV). This gives a kind of impression (at the scale of the plots) that a unique regression line might describe the 4 sets of data. On the other hand, with large amount of HF exchange (global or range-separated hybrids), the intercepts at the origin are

systematically larger for the $\Delta E_{S_0-S_1}$ values than the $\Delta E_{S_0-T_1}$ ones. In addition, for the triplets, there is a difference between the TD-DFT and TD-DFT/TDA results, with smaller intercepts at the origin using the TD-DFT scheme.

These results substantiate our findings in the previous sections. The functionals that tend to predict the vertical singlet and triplet excitation energies better, give better correlations to the riCC2 results. The Tamm–Dancoff approximation again gives improved results for the vertical triplet excitation energies, proving that, owing to correcting for the errors related to triplet instabilities,[58] it is a very useful approximation to get the most accurate results from the TD-DFT calculations.

4 Conclusions

In this work, the adiabatic TD-DFT method has been employed to evaluate the first singlet and triplet excitation energies and the corresponding singlet–triplet energy gaps on a set of 10 compounds that were designed to exhibit thermally activated delayed fluorescence. These compounds have been selected because they cover a broad range of singlet–triplet energy splitting values, together with fluorescence characteristics going from blue to red, while presenting a clear chemical diversity in terms of donor and acceptor units. By using a broad variety of XC functionals, our goal was to highlight the best ones in comparison to benchmark results evaluated at the resolution-of-the-identity second-order coupled cluster (riCC2) level, while the performance of the latter method against experimental data was preliminarily demonstrated.

We have shown that two functionals stand out when aiming at predicting the vertical singlet and triplet excitation energies, being LC-BLYP20 and M06-2X. These functionals show steady behavior and minimal errors on the excited state energies in comparison to riCC2 calculations. LC-BLYP20 tends to predict the singlet energies more accurately than the triplet energies, whereas the opposite is true for M06-2X. Therefore, the singlet–triplet energy gaps that follow from these calculations have similar errors for a given compound. Furthermore, when looking at the singlet–triplet energy gaps, LC-ωPBE17 and LC-BLYP17 outperform LC-BLYP20 and M06-2X. The question of which functional is best to use then falls back to the primary focus of the investigation. If the focus is on the singlet state energies, LC-BLYP20 followed by LC-ωPBE17 and LC-BLYP17 would be the optimal functionals. If the focus is rather on the position of the triplet states and their mutual energy difference, M06-2X would be the optimal functional. Using the Tamm–Dancoff approximation has no significant influence on the singlet excitation energies. It does, however, decrease the errors obtained using LC-BLYP20, LC-BLYP17, LC-ωPBE17, and M06-2X for the triplet excitation energies and consequently for the singlet–triplet energy gap. Furthermore, using TDA increases the precision of the obtained triplet energy errors within the set of 10 compounds. Although we have shown in this work that small errors for the singlet–triplet energy gap can be obtained with a large number of functionals, their accuracy lies in a cancellation of two large errors. These functionals are therefore not trustworthy.

We therefore propose the use of the Tamm–Dancoff approximation in combination with either LC-BLYP17, LC-ωPBE17, LC-BLYP20, or M06-2X when looking at the ΔE_{ST} quantities for a given compound. Ultimately, a hybrid approach using the TDA approach and taking the ΔE_{ST} from the singlet and triplet excitation energies obtained with LC-BLYP20 and M06-2X, respectively, gives errors on the singlet–triplet gap that are roughly the same as those obtained with the best functional LC-BLYP17, but with better estimates for the singlet and triplet excitation energies respectively.

Conflicts of interest

The authors declare no competing financial interest.

Acknowledgements

This work is supported by the University of Namur and Hasselt University (PhD BILA scholarship T. Cardeynaels). The authors also thank the Research Foundation – Flanders (FWO Vlaanderen) for financial support (project G.0877.18N, Hercules project GOH3816NAUHL, and SB PhD scholarship S. Paredis). The calculations were performed on the computers of the ''Consortium des équipements de Calcul Intensif (CÉCI)'' (http://www.ceci-hpc.be), including those of the ''UNamur Technological Platform of High-Performance Computing (PTCI)'' (http://www.ptci.unamur.be), for which we gratefully acknowledge the financial support from the FNRS-FRFC, the Walloon Region, and the University of Namur (Conventions No. 2.5020.11, GEQ U.G006.15, U.G018.19, 1610468, and RW/GEQ2016).

References

1 A. Endo, M. Ogasawara, A. Takahashi, D. Yokoyama, Y. Kato and C. Adachi, *Adv. Mater.*, 2009, **21**, 4802–4806.
2 J. Guo, Z. Zhao and B. Z. Tang, *Adv. Opt. Mater.*, 2018, **6**, 1800264.
3 T. Huang, W. Jiang and L. Duan, *J. Mater. Chem. C*, 2018, **6**, 5577–5596.
4 Y. Liu, C. Li, Z. Ren, S. Yan and M. R. Bryce, *Nat. Rev. Mater.*, 2018, **3**, 18020.
5 Y. Tao, K. Yuan, T. Chen, P. Xu, H. Li, R. Chen, C. Zheng, L. Zhang and W. Huang, *Adv. Mater.*, 2014, **26**, 7931–7958.
6 Q. Wei, N. Fei, A. Islam, T. Lei, L. Hong, R. Peng, X. Fan, L. Chen, P. Gao and Z. Ge, *Adv. Opt. Mater.*, 2018, **6**, 1800512.
7 M. Y. Wong and E. Zysman-Colman, *Adv. Mater.*, 2017, **29**, 1605444.
8 Z. Yang, Z. Mao, Z. Xie, Y. Zhang, S. Liu, J. Zhao, J. Xu, Z. Chi and M. P. Aldred, *Chem. Soc. Rev.*, 2017, **46**, 915–1016.

9 K. Kawasumi, T. Wu, T. Zhu, H. S. Chae, T. Van Voorhis, M. A. Baldo and T. M. Swager, *J. Am. Chem. Soc.*, 2015, **137**, 11908–11911.

10 J. Lee, K. Shizu, H. Tanaka, H. Nomura, T. Yasuda and C. Adachi, *J. Mater. Chem. C*, 2013, **1**, 4599–4604.

11 G. Mehes, H. Nomura, Q. Zhang, T. Nakagawa and C. Adachi, *Angew. Chem., Int. Ed.*, 2012, **51**, 11311–11315.

12 P. L. Santos, J. S. Ward, P. Data, A. S. Batsanov, M. R. Bryce, F. B. Dias and A. P. Monkman, *J. Mater. Chem. C*, 2016, **4**, 3815–3824.

13 M. Baba, *J. Phys. Chem. A*, 2011, **115**, 9514–9519.

14 M. A. El-Sayed, *J. Chem. Phys.*, 1963, **38**, 2834–2838.

15 F. B. Dias, J. Santos, D. R. Graves, P. Data, R. S. Nobuyasu, M. A. Fox, A. S. Batsanov, T. Palmeira, M. N. Berberan-Santos, M. R. Bryce and A. P. Monkman, *Adv. Sci.*, 2016, **3**, 1600080.

16 J. Eng and T. J. Penfold, *Chem. Rec.*, 2020, 1–27, DOI: 10.1002/tcr.202000013,.

17 M. K. Etherington, J. Gibson, H. F. Higginbotham, T. J. Penfold and A. P. Monkman, *Nat. Commun.*, 2016, **7**, 13680.

18 J. Gibson, A. P. Monkman and T. J. Penfold, *ChemPhysChem*, 2016, **17**, 2956–2961.

19 T. J. Penfold, F. B. Dias and A. P. Monkman, *Chem. Commun.*, 2018, **54**, 3926–3935.

20 X. K. Chen, D. Kim and J. L. Brédas, *Acc. Chem. Res.*, 2018, **51**, 2215–2224.

21 T. J. Penfold, E. Gindensperger, C. Daniel and C. M. Marian, *Chem. Rev.*, 2018, **118**, 6975–7025.

22 P. K. Samanta, D. Kim, V. Coropceanu and J. L. Brédas, *J. Am. Chem. Soc.*, 2017, **139**, 4042–4051.

23 J. Sanz-Rodrigo, Y. Olivier and J.-C. Sancho-García, *Molecules*, 2020, **25**, 1006.

24 J.-M. Mewes, *Phys. Chem. Chem. Phys.*, 2018, **20**, 12454–12469.

25 Y. Olivier, J. C. Sancho-Garcia, L. Muccioli, G. D'Avino and D. Beljonne, *J. Phys. Chem. Lett.*, 2018, **9**, 6149–6163.

26 D. Jacquemin, E. A. Perpète, I. Ciofini and C. Adamo, *J. Chem. Theory Comput.*, 2010, **6**, 1532–1537.

27 A. D. Laurent, C. Adamo and D. Jacquemin, *Phys. Chem. Chem. Phys.*, 2014, **16**, 14334–14356.

28 B. M. Wong and J. G. Cordaro, *J. Chem. Phys.*, 2008, **129**, 214703.

29 C. Brückner and B. Engels, *Chem. Phys.*, 2017, **482**, 319–338.

30 S. Huang, Q. Zhang, Y. Shiota, T. Nakagawa, K. Kuwabara, K. Yoshizawa and C. Adachi, *J. Chem. Theory Comput.*, 2013, **9**, 3872–3877.

31 T. J. Penfold, *J. Mater. Chem. C*, 2015, **119**, 13535–13544.

32 H. Sun, C. Zhong and J. L. Brédas, *J. Chem. Theory Comput.*, 2015, **11**, 3851–3858.

33 M. Moral, L. Muccioli, W. J. Son, Y. Olivier and J. C. Sancho-Garcia, *J. Chem. Theory Comput.*, 2015, **11**, 168–177.

34 J. P. Perdew and K. Schmidt, *AIP Conf. Proc.*, 2001, **577**, 1–20.

35 L. Kronik, T. Stein, S. Refaely-Abramson and R. Baer, *J. Chem. Theory Comput.*, 2012, **8**, 1515–1531.

36 C. Hättig and F. Weigend, *J. Chem. Phys.*, 2000, **113**, 5154–5161.

37 Y. Kaizu, H. Maekawa and H. Kobayashi, *J. Phys. Chem.*, 1986, **90**, 4234–4238.

38 W. Ni, G. G. Gurzadyan, J. Zhao, Y. Che, X. Li and L. Sun, *J. Phys. Chem. Lett.*, 2019, **10**, 2428–2433.

39 X. Miao, W. Hu, T. He, H. Tao, Q. Wang, R. Chen, L. Jin, H. Zhao, X. Lu, Q. Fan and W. Huang, *Chem. Sci.*, 2019, **10**, 3096–3102.

40 J. Zhao, K. Xu, W. Yang, Z. Wang and F. Zhong, *Chem. Soc. Rev.*, 2015, **44**, 8904–8939.

41 K. Plaetzer, B. Krammer, J. Berlanda, F. Berr and T. Kiesslich, *Lasers Med. Sci.*, 2009, **24**, 259–268.

42 S. Ji, J. Ge, D. Escudero, Z. Wang, J. Zhao and D. Jacquemin, *J. Org. Chem.*, 2015, **80**, 5958–5963.

43 J. Zhao, K. Chen, Y. Hou, Y. Che, L. Liu and D. Jia, *Org. Biomol. Chem.*, 2018, **16**, 3692–3701.

44 C. Y. Chan, L. S. Cui, J. U. Kim, H. Nakanotani and C. Adachi, *Adv. Funct. Mater.*, 2018, **28**, 1706023.

45 F. Ni, Z. Wu, Z. Zhu, T. Chen, K. Wu, C. Zhong, K. An, D. Wei, D. Ma and C. Yang, *J. Mater. Chem. C*, 2017, **5**, 1363–1368.

46 P. Rajamalli, N. Senthilkumar, P. Gandeepan, C. C. Ren-Wu, H. W. Lin and C. H. Cheng, *ACS Appl. Mater. Interfaces*, 2016, **8**, 27026–27034.

47 B. Zhao, G. Xie, H. Wang, C. Han and H. Xu, *Chemistry*, 2019, **25**, 1010–1017.

48 H.-Y. Liu, P.-J. Wu, S.-Y. Kuo, C.-P. Chen, E.-H. Chang, C.-Y. Wu and Y.-H. Chan, *J. Am. Chem. Soc.*, 2015, **137**, 10420–10429.

49 Y. Zhao and D. G. Truhlar, *Theor. Chem. Acc.*, 2008, **120**, 215–241.

50 G. W. T. M. J. Frisch, H. B. Schlegel, G. E. Scuseria, M. A. Robb, J. R. Cheeseman, G. Scalmani, V. Barone, B. Mennucci, G. A. Petersson, H. Nakatsuji, M. Caricato, X. Li, H. P. Hratchian, A. F. Izmaylov, J. Bloino, G. Zheng, J. L. Sonnenberg, M. Hada, M. Ehara, K. Toyota, R. Fukuda, J. Hasegawa, M. Ishida, T. Nakajima, Y. Honda, O. Kitao, H. Nakai, T. Vreven, J. A. Montgomery, Jr., J. E. Peralta, F. Ogliaro, M. Bearpark, J. J. Heyd, E. Brothers, K. N. Kudin, V. N. Staroverov, T. Keith, R. Kobayashi, J. Normand, K. Raghavachari, A. Rendell, J. C. Burant, S. S. Iyengar, J. Tomasi, M. Cossi, N. Rega, J. M. Millam, M. Klene, J. E. Knox, J. B. Cross, V. Bakken, C. Adamo, J. Jaramillo, R. Gomperts, R. E. Stratmann, O. Yazyev, A. J. Austin, R. Cammi, C. Pomelli, J. W. Ochterski, R. L. Martin, K. Morokuma, V. G. Zakrzewski, G. A. Voth, P. Salvador, J. J. Dannenberg, S. Dapprich, A. D. Daniels, O. Farkas, J. B. Foresman, J. V. Ortiz, J. Cioslowski and D. J. Fox, Gaussian, Inc., Wallingford CT, 2016.

51 TURBOMOLE V7.4 2019, a development of University of Karlsruhe and Forschungszentrum Karlsruhe GmbH, 1989–2007, TURBOMOLE GmbH, since 2007, available from http://www.turbomole.com.

52 M. Schreiber, M. R. Silva-Junior, S. P. Sauer and W. Thiel, *J. Chem. Phys.*, 2008, **128**, 134110.

53 A. Hellweg, S. A. Grün and C. Hättig, *Phys. Chem. Chem. Phys.*, 2008, **10**, 4119–4127.

54 D. Jacquemin, I. Duchemin and X. Blase, *J. Chem. Theory Comput.*, 2015, **11**, 5340–5359.

55 A. Tajti and P. G. Szalay, *J. Chem. Theory Comput.*, 2019, **15**, 5523–5531.
56 J.-D. Chai and M. Head-Gordon, *Phys. Chem. Chem. Phys.*, 2008, **10**, 6615–6620.
57 Q. Zhang, B. Li, S. Huang, H. Nomura, H. Tanaka and C. Adachi, *Nat. Photonics*, 2014, **8**, 326–332.
58 M. J. G. Peach and D. J. Tozer, *J. Phys. Chem. A*, 2012, **116**, 9783–9789.
59 B. Moore, H. Sun, N. Govind, K. Kowalski and J. Autschbach, *J. Chem. Theory Comput.*, 2015, **11**, 3305–3320.
60 M. Miura, Y. Aoki and B. Champagne, *J. Chem. Phys.*, 2007, **127**, 084103.
61 M. J. Peach, M. J. Williamson and D. J. Tozer, *J. Chem. Theory Comput.*, 2011, **7**, 3578–3585.
62 B. Moore Ii, R. L. Schrader, K. Kowalski and J. Autschbach, *ChemistryOpen*, 2017, **6**, 385–392.